Electronic Research Archive

ERA, 31(6): 3510–3533.
DOI: 10.3934/era.2023178
Received: 26 February 2023
Revised: 06 April 2023
Accepted: 12 April 2023
Published: 21 April 2023

http://www.aimspress.com/journal/ERA

Research article

Effect of graphene on the properties of epoxy in hygrothermal environment by molecular dynamics method

Xiuli Zhang[1,2,3], Guangming He[2], Hui Yao[3], Xuanxi Wang[2], Guoru Ma[2], Junliang Li[2], Zulong Yu[2], Guozhong Lu[2] and Zhifei Gao[4,*]

[1] State Key Laboratory of Solid Waste Reuse for Building Materials, Beijing Building Materials Academy of Sciences Research, Beijing 100041, China
[2] Beijing Building Materials Testing Academy Co., Ltd. Beijing 100041, China
[3] Faculty of Architecture, Civil and Transportation Engineering, Beijing University of Technology, Beijing 100124, China
[4] National Center for Materials Service Safety, University of Science and Technology Beijing, Beijing 100083, China

* **Correspondence:** Email: zf_g123@126.com.

Abstract: The physical and mechanical properties of graphene-reinforced epoxy (epoxy/graphene) in hygrothermal environment need to be comprehensively understood. This is because it is necessary to predict the durability of epoxy/graphene when epoxy/graphene is used in an aggressive environment with high humidity and high temperature. Based on the molecular dynamics method, the influences of water content (2, 4 and 6%) and temperature (298, 333 and 368 K) on the physical and tensile properties of epoxy/graphene were studied in this research. The results showed that after the addition of graphene, the free volume fraction of epoxy and the diffusion coefficient of water molecules in the epoxy decreased, and the density, tensile strength and deformation performance of epoxy increased. In the hygrothermal environment, the tensile strength degradation rate of epoxy/graphene was lower than that of pure epoxy. The failure mechanism and mechanical response of epoxy/graphene during the tensile process in the nanoscale were revealed. The research results provide a reference for the design and performance optimization of epoxy/graphene composites in a hygrothermal environment.

Keywords: molecular dynamics; graphene; epoxy; physical properties; tensile properties

1. Introduction

Epoxy has many advantages, such as excellent mechanical properties, adhesion and chemical resistance, low density, and low cost [1–4]. Therefore, it has been widely applied in civil engineering, aerospace, electronics, and other fields [5,6]. However, when pure epoxy was used in a hygrothermal environment, the basic properties of the epoxy significantly decreased [7–10]. Uthaman et al. [11] investigated the properties of epoxy aging in water. The results indicated that after immersing the epoxy in water at 20, 40, and 60 ℃ for 80 days, the glass transition temperature of epoxy decreased by 8.0, 6.8 and 3.4%, the tensile strength decreased by 4.2, 23.9 and 41.8%, and the elastic modulus decreased by 7.3, 11.0, and 13.3%, respectively. The results of research conducted by Wang et al. [12] showed that the tensile strength of epoxy decreased by 24 and 28% after immersing the epoxy in water at 20 and 60 ℃ for one month. Jeyranpour et al. [13] used the molecular dynamics method to study the influence of temperature on the properties of epoxy. The results revealed that as the temperature increased, the density, elastic modulus, bulk modulus, and shear modulus decreased, and the free volume increased.

When epoxy was exposed to a hygrothermal environment, the physical and mechanical properties decreased, resulting in a reduction of service life [10,14,15]. In recent years, polymer composites have become increasingly used in various engineering fields, so improving the physical and mechanical properties of pure epoxy in a hygrothermal environment is urgent [15,16]. The properties of epoxy can be improved by adding different nanofillers. Monolithic graphene was an ideal filler for polymer nanocomposites [17,18] because of its excellent mechanical properties. For example, the Young's modulus and tensile strength of graphene are up to 1100 and 130 GPa. Graphene in carbon nanomaterials has become a research hotspot in the composite materials field [19,20].

Some researchers have investigated the mechanical properties of epoxy/graphene in a dry environment and at room temperature. The results of the study by Ni et al. [21] showed that when the content of graphene filler in the three-dimensional epoxy/graphene was 0.2 wt%, the tensile strength and compressive strength of epoxy increased by 120.9 and 148.3%, respectively. Hu et al. [22] conducted the tensile experiment of graphene oxide-reinforced epoxy. It was found that when the mass fraction of graphene oxide was 0.1%, the tensile strength and tensile modulus of the composite were 26.60 and 21.69% higher than those of pure epoxy, respectively. Xiao et al. [23] studied the tensile performance of graphene-enhanced epoxy, and the results showed that when the graphene oxide content was 2%, the tensile strength and elastic modulus of the composite increased by 50 and 19.6%, respectively. Yao et al. [24] found that compared with pure epoxy, the tensile strength and elongation at break for the epoxy/graphene composites with 0.8 wt% graphene increased by 37 and 63%, respectively, and Young's modulus did not decrease. Bansal et al. [25] investigated the effect of graphene oxide (GO) on the mechanical properties of the epoxy/GO at different GO wt% values. The results showed that the elastic modulus and the hardness of epoxy/GO increased with the increasing graphene oxide percentage, and the best improvement was observed when the graphene oxide percentage was 1 wt%. Hu et al. [26] tested the flexural properties of epoxy/graphene, and the results showed that when the mass fraction of the filler material was 3%, the flexural modulus and flexural strength increased by 19.1 and 62.1%, respectively. The experiment conducted by Zhang et al. [27] indicated that the addition of 0.5 wt% graphene oxide increased the tensile strength and flexural strength of the epoxy composite by 80 and by 49%, respectively. The experiment carried out by Wolk et al. [28] showed that the addition of 0.5 wt% graphene oxide improved the deformation of epoxy from 2.5 to 3.1 mm. The experiment conducted by Her and Chen [29] reported that the elastic modulus

and ultimate tensile strength of epoxy/GNP (graphene nanoplatelet) nanocomposites with 1 wt% GNPs were 40.7 and 25.8% higher than those of pure epoxy. Bian et al. [30,31] investigated the mechanical properties of graphene reinforced epoxy using the molecular dynamics (MD) method and finite element method (FEM). The results showed that the mechanical performance of composites was influenced by the graphene volume fraction and graphene direction. The graphene showed a great potential in improving the tensile strength of the composite.

In actual engineering, epoxy/graphene was inevitably used in high humidity and temperature environments, so understanding the influence of temperature and water molecules on its performance is crucial. Yadav et al. [32] investigated the effect of the functionalization of graphene on the glass transition temperature of epoxy, and it was revealed that the introduced graphene increased the transition temperature of the composite. Salehi and Rash-Ahmadi [33] reported that Young's modulus and tensile strength of nanocomposites increased with the increasing graphene oxide weight percentage, and Young's modulus decreased with the increasing temperature. Some previous research has been conducted on the water absorption property of epoxy/graphene. Starkova et al. [34] reported an aging test on epoxy/graphene in a water environment and found that the diffusion rate of water molecules in epoxy/graphene was obviously lower than that in pure epoxy. Prolongo et al. [35] studied the effects of graphene transverse size and thickness on the water absorption property of epoxy. The results indicated that after adding graphene to the epoxy, the water absorption rate decreased, and the influence of water molecules on the flexural properties of epoxy/graphene was lower than that of pure epoxy. Li et al. [36] investigated the anticorrosion properties of graphene (GN)- or graphene oxide (GO)-reinforced epoxy (EP) coatings using a molecular dynamics method. The results showed that the introduced GN or GO increased the compactness of the epoxy. At high temperatures, the free volume fractions of GN/EP or GO/EP were lower than that of the pure epoxy. The added GO had a barrier effect on the diffusion of water molecules. Zhu et al. [37] performed the aging experiment of epoxy composite coatings reinforced with reduced graphene oxide (RGO) nanosheets in 10.0 wt% NaCl solution at 80 °C. The results indicated that the proper addition of RGO nanosheets effectively increased the adhesion and toughness of the epoxy composite coatings and reduced the number and the size of pores in the epoxy composite coatings. The epoxy composite coating with 1.0 wt% RGO showed the best anti-corrosion performance.

The existing studies on epoxy/graphene in hygrothermal environment mainly focused on its physical properties. However, when epoxy/graphene materials bear loads in civil engineering, it is necessary to comprehensively understand its long-term performance under severe conditions, especially the mechanical properties in a hygrothermal environment. However, the research on the degradation process and nanoscopic degradation mechanism of epoxy/graphene in a hygrothermal environment has still been relatively weak [38], which has hindered its application in engineering. Due to the limitations of experiments, the numerical methods of FEM and MD have been widely used in the study of composite properties. The FEM is usually used in microscale, and the MD method is usually used in nanoscale [39,40].

Molecular dynamics simulations play a crucial role in complementing experimental studies in the field of epoxy and reinforced epoxy research [1,2]. The study conducted by [30,31] indicated that molecular dynamics simulations successfully predicted the properties of epoxy and epoxy/graphene. Molecular dynamics simulations provide valuable insights into material behavior at the atomic level, which can be challenging to obtain through experimental methods alone [41]. The use of molecular dynamics methods for studying epoxy materials offers several advantages. These simulations allow

for the observation of material behavior at the atomic level, enabling the calculation of various properties that can be difficult to measure experimentally. Molecular dynamics simulations make it possible to observe the evolution of atoms and molecules, and find out the source for certain phenomena observed at the macrolevel [31,42–45]. Additionally, compared with traditional experimental research, molecular dynamics simulations reduced the time-consuming cycle and the cost of new materials, obviously [46].

Based on the molecular dynamics method, this study investigated the degradation process of epoxy/graphene in a hygrothermal environment at the molecular level and analyzed the effects of water content and temperature on the physical and tensile properties of epoxy/graphene. The results revealed the degradation mechanism of epoxy/graphene, and provide a profound understanding of the enhancement mechanism of graphene on the corrosion resistance of epoxy.

2. Simulation method

The epoxy model was constructed through the crosslinking reaction between the diglycidyl ether of bisphenol A (DGEBA) and the curing agent hexahydro-4-methylphthalic anhydride (MeHHPA). The crosslinking reaction was the process of forming a three-dimensional network structure using a linear structure with active atoms through the chemical reaction.

2.1. Establishment of the monomer molecular model

First, the two-dimensional structure models of DGEBA and MeHHPA monomers were established. The reasonable three-dimensional structure models were obtained by conducting the geometric optimization and are shown in Figures 1 and 2. Then, the active reaction atoms C and O on the DGEBA molecules were named R1 and R3, and the active reaction atoms O and C on the MeHHPA molecules were named R2 and R4. The reaction atom pairs were R1 and R2, R3 and R4, respectively.

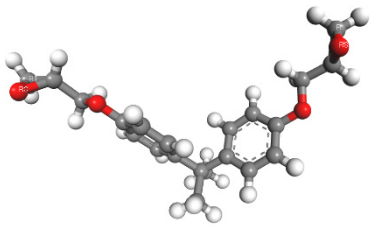

Figure 1. Monomer molecular model of DGEBA.

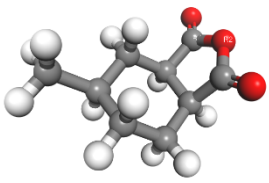

Figure 2. Monomer molecular model of MeHHPA.

2.2. Construction of the uncrosslinked model

In this paper, the COMPASS II force field was employed in the molecular dynamics simulation process. Andersen and Berendsen's methods were applied to control the system temperature and pressure. Atom-based and Ewald simulation methods were used in the van der Waals force and electrostatic interaction, respectively.

The amorphous models of pure epoxy and epoxy/graphene are shown in Figures 3 and 4, and they contained 36 DGEBA molecules and 72 MeHHPA molecules. The size of the uncrosslinked pure epoxy model was 34 Å × 34 Å × 29.17 Å. The size of the graphene sheet was 30 Å × 30 Å. The number of carbon atoms in the graphene was 336. The graphene sheet was end grafted by adding hydrogen atoms, and was located in the middle of the epoxy resin. The size of the uncrosslinked epoxy/graphene model was 34 Å × 34 Å × 34 Å. Every amorphous model performed 2000 steps of geometric optimization to achieve the minimum energy. In the models, the red ball representes the oxygen atom (O), the gray ball represents the carbon atom (C), and the white ball represents the hydrogen atom (H).

The geometrically optimized models performed full relaxation dynamics in constant volume and temperature (NVT) ensemble for 50 ps at 298 K with a time step of 1 fs. After that, the system was equilibrated in constant pressure and temperature (NPT) ensemble for 50 ps at 101 kPa. Finally, the stable uncrosslinked systems were obtained.

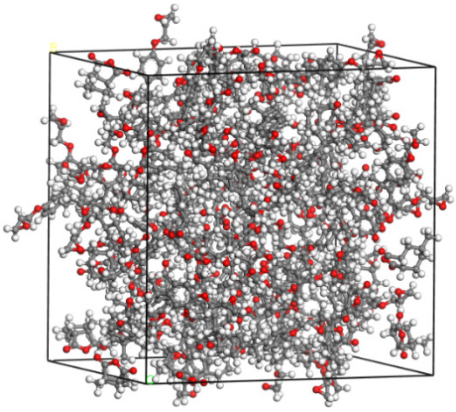

Figure 3. The uncrosslinked model of pure epoxy.

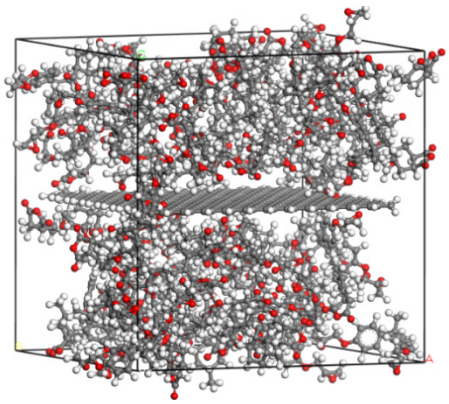

Figure 4. The uncrosslinked model of epoxy/graphene.

2.3. Construction of the crosslinked model

According to the crosslinked reaction mechanism between DGEBA and MeHHPA, a script program was utilized to realize the crosslinking of the epoxy system. The truncation radius was set to 3.5–7.5 Å, and the step size was 1 Å [44,47]. The crosslinking temperature of the model was 298 K, and the target crosslinking degree was 100%. First, the distance between the reaction atom pairs was measured. If the distance was less than the set crosslinking radius, the bonds that connected to the reaction atoms were broken, and a new covalent bond formed between the reaction atoms of R1 and R2, or between the reaction atoms of R3 and R4, as shown in Figure 5. Second, the crosslinking system was geometrically optimized for 2000 steps. The geometrically optimized models performed full relaxation dynamics in NVT (T = 298 K) ensemble for 50 ps with a time step of 1 fs. Subsequently, the system was simulated in NPT (T = 298 K, P = 101 kPa) ensemble for 50 ps. The above two steps were repeated in the new equilibrium system until no new bonds were created or the number of crosslinking reactions reached four times. Third, the truncation radius was increased. Then, the three processes (formation of covalent bonds, geometric optimization, and dynamic equilibrium) were repeated until the predetermined truncation radius or the crosslinking degree reached the set value, and the crosslinking process ended at this moment. Then, the crosslinked epoxy system was applied in the NVT ensemble and NPT ensemble for 500 ps with a time step of 1 fs, respectively. The temperature was 298 K, and the pressure was 101 kPa [48]. Finally, the stable models were obtained as shown in Figures 6 and 7.

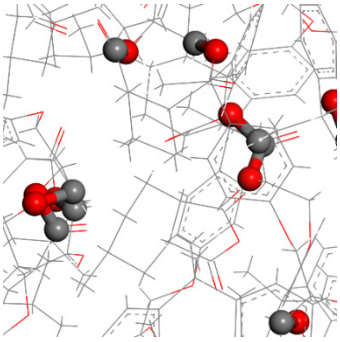

Figure 5. Formation of new bonds in epoxy model.

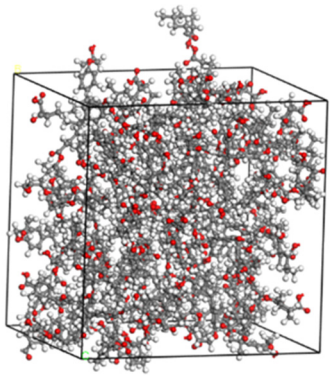

Figure 6. The crosslinked epoxy model.

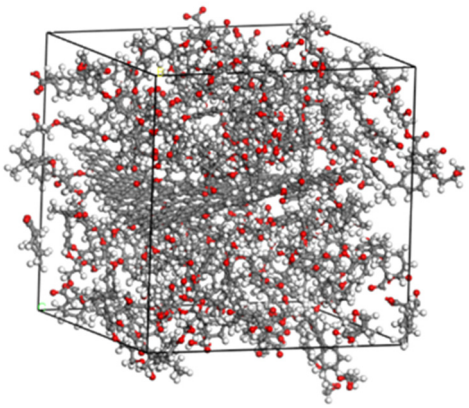

Figure 7. The crosslinked epoxy/graphene model.

2.4. The epoxy models and epoxy/graphene models in a water environment

Jin et al. [49] conducted a water absorption test on epoxy and reported that the saturated moisture content of the epoxy on the 5th day was 6.557%. According to the experiment results, the maximum water content of the epoxy and epoxy/graphene models built in this work was set to 6%. Based on the models built in Section 2.3, different numbers of water molecules were added to the models to build the moist epoxy models and the moist epoxy/graphene models. The water contents of the models were 0, 1, 2, 3, 4, 5 and 6%, respectively. These models were geometrically optimized and relaxed using the dynamics method in Section 2.2 to reach stable states as shown in Figures 8 and 9.

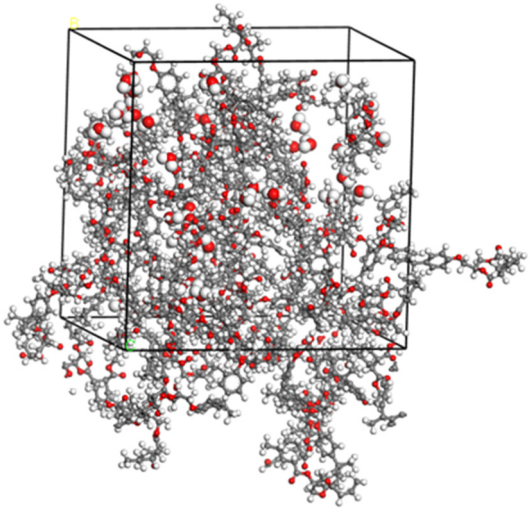

Figure 8. The epoxy model with a water content of 4%.

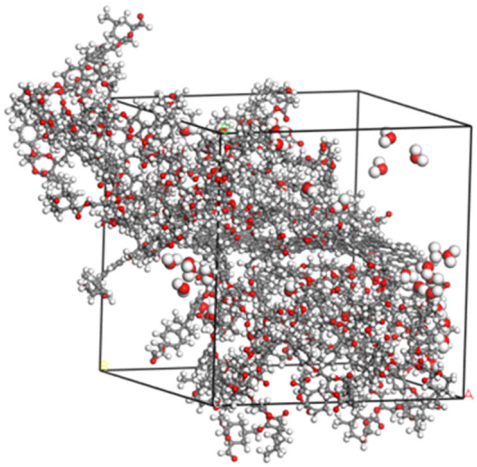

Figure 9. The epoxy/graphene model with a water content of 4%.

3. Results and discussion

3.1. The density and volume

The densities of pure epoxy and epoxy/graphene systems with different water contents at 298 K are shown in Table 1, and the density of pure epoxy in the dry environment was 1.1194 g/cm^3. The density of the epoxy in the experiment conducted by Li [7] was about 1.2 g/cm^3 which verifies the rationality of the models in the paper. The changes in density with water content are shown in Figure 10.

Table 1. The densities of the models.

Model	Water content/%	Density/(g/cm^3)	Model	Water content/%	Density/(g/cm^3)
EP0	0	1.1194	EP/GN0	0	1.1870
EP1	1	1.1251	EP/GN1	1	1.1882
EP2	2	1.1247	EP/GN2	2	1.1880
EP3	3	1.1119	EP/GN3	3	1.1784
EP4	4	1.1066	EP/GN4	4	1.1751
EP5	5	1.1048	EP/GN5	5	1.1744
EP6	6	1.0982	EP/GN6	6	1.1688

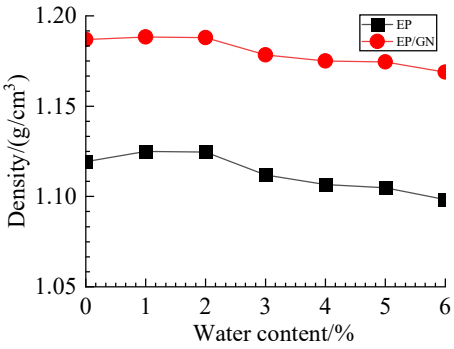

Figure 10. Effect of the water content on density.

It was observed that when the water content of the models was less than 2%, the densities of the moist models were lower than that of the dry model. When the water content of the models was higher than 2%, the density decreased with the increase in water content.

When the water molecules were added to the systems, hydrogen bonds were formed between water molecules and polar groups of the epoxy resin, as well as between water molecules themselves. The intermolecular hydrogen bonding force was higher than the van der Waals force, and thus the formation of hydrogen bonds had a significant impact on the system's properties [50]. The number of hydrogen bonds in each system was calculated, as shown in Figure 11. EP-WP represented the hydrogen bonds connected to epoxy resin (the sum of hydrogen bonds between water molecules and polar groups and hydrogen bonds between polymer molecules themselves). EP/GN-WP represented the hydrogen bonds connected to epoxy/graphene. EP-WW and EP/GN-WW represented the hydrogen bonds between water molecules themselves in epoxy and epoxy/graphene, respectively.

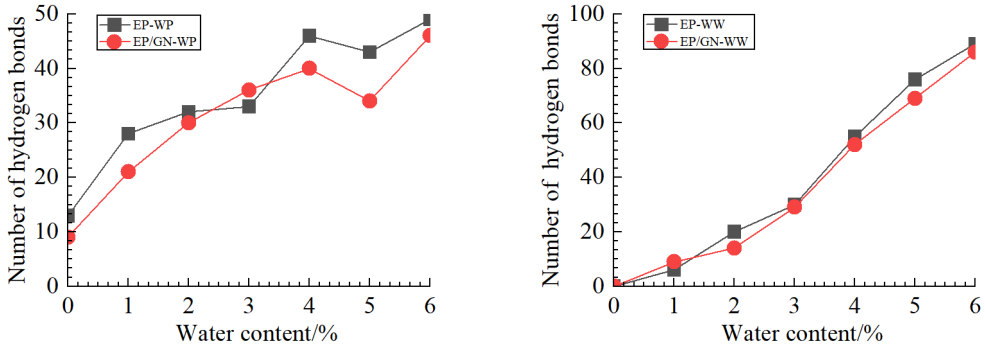

(a) Hydrogen bonds connected to epoxy resin (b) Hydrogen bonds between water molecules

Figure 11. Hydrogen bonds.

Overall, as the water content increased, the number of hydrogen bonds connecting to epoxy resin molecules increased, and the number of hydrogen bonds between water molecules also increased. In the initial stage of moisture absorption, hydrogen bonds connected to epoxy resin played a dominant role, which was consistent with the research results of Liu [51]. The increase of the binding force between water molecules and polar groups of the epoxy resin made the material structure denser. When

the water content of the systems was higher than 3%, the increase rate of the number of hydrogen bonds between water molecules significantly accelerated. As the water content increased, the plasticizing effect of water molecules became more obvious.

Free volume fraction was the ratio of free volume to the total volume of the system as shown in Eq (1). The higher the free volume fraction is, the faster the motility of the molecular chains, and the worse the static properties of the system [52].

$$\mathrm{FFV} = \frac{V}{V + V_0} \tag{1}$$

where V represents the volume of the cavity, and V_0 represents the volume occupied by the molecular chains.

The schematic diagram of the free volume of the model is shown in Figure 12. The blue area represents the free volume. The gray area represents the coatings of the free volume. The change of free volume fraction with water content is shown in Figure 13.

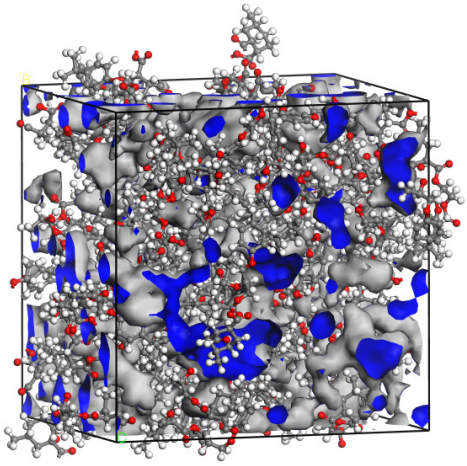

Figure 12. Schematic illustration of the free volume.

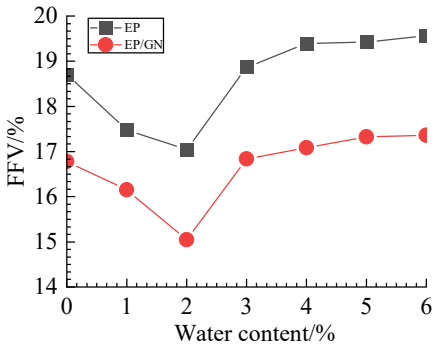

Figure 13. Effect of the water content on the free volume fraction.

Figure 13 shows that when the water content of the models was lower than 2%, with the increase

in water content, the free volume fraction decreased. This was due to the addition of water molecules to the system that resulted in more hydrogen bonds, and thus the intermolecular forces increased. When the water content of the models was higher than 2%, with the increase in water content, the free volume fraction increased. That was due to the addition of water molecules, causing the plasticization of the system.

Figures 10 and 13 illustrate that, as the water content increased, the trends of density and free volume fraction of pure epoxy were similar to that of epoxy/graphene. The addition of graphene increased the density of the system. The influences of water molecules on the density and free volume fraction of the epoxy/graphene were relatively lower. One reason was that the addition of graphene reduced the porosity of the epoxy. The other reason was that the attraction of graphene to the epoxy reduced the volume expansion of the epoxy.

3.2. The diffusion of water molecules

When the epoxy was in the hygrothermal environment, the free water molecules entered the resin through the diffusion process, which induced the change of physical and mechanical properties of the epoxy. Thus, it was necessary to study the effect of graphene on the diffusion process of water molecules in epoxy. The diffusion of water molecules could be characterized by the diffusion coefficient (D) [53], shown in Eq (2).

$$D=\frac{1}{6}\lim_{t\to\infty}\frac{d}{dt}\left\langle\left[\vec{r}(t)-\vec{r}(0)\right]^2\right\rangle \tag{2}$$

where $r(t)$ and $r(0)$ represented the displacements of atoms at the moment t and 0, respectively; < > is the average value of the displacement of all the atoms.

The mean square displacement (MSD) shown in Eq (3) could indicate the motion characteristics of the particles. The higher the MSD was, the faster the particle moved. The system diffusion coefficient D was related to the slope of the MSD curve as shown in Eq (4).

$$\text{MSD}=\left\langle\left[\vec{r}(t)-\vec{r}(0)\right]^2\right\rangle \tag{3}$$

$$D=\frac{1}{6}\text{MSD} \tag{4}$$

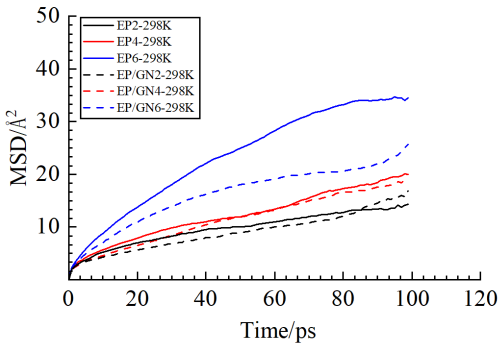

Figure 14. MSD of the water molecules in the systems with different water contents.

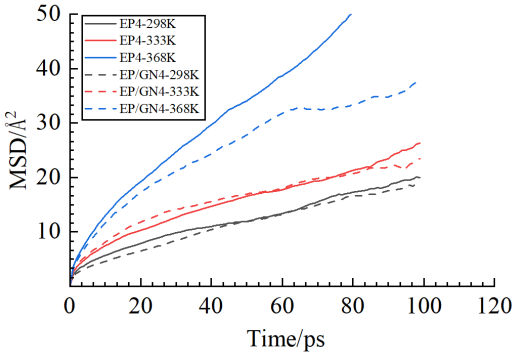

Figure 15. MSD of the water molecules in the systems at different temperatures.

Figure 14 shows the MSD of water molecules in the systems with different water contents at 298 K. It was concluded that the diffusion coefficient of water molecules in the systems increased with the increase of water content. When the water contents were 2 and 4%, the addition of graphene had little effect on the diffusion coefficient of water molecules. When the water content was 6%, the diffusion rate of water molecules in epoxy/graphene was significantly lower than that in pure epoxy.

Figure 15 shows the MSD of water molecules in the systems with a water content of 4% at different temperatures. It demonstrates that the diffusion coefficient of water molecules in the system increased with the increasing temperature. The diffusion coefficients of water molecules in the epoxy/graphene and pure epoxy were similar when the temperatures were 298 and 333 K. At 368 K, the addition of graphene significantly reduced the diffusion rate of water molecules in the epoxy because the presence of graphene hindered the diffusion of water molecules. It was concluded that in the high humidity or high-temperature environment, the addition of graphene had a significant effect on reducing the diffusion of water molecules in the systems.

3.3. Tensile behavior

In order to study the influence of graphene on the tensile behavior of epoxy in the hygrothermal environment, five pure epoxy (EP) models and five epoxy/graphene (EP/GN) models were constructed. The open-source code Large-scale Atomic/Molecular Massively Parallel Simulator (LAMMPS) was used in the molecular dynamics simulation. The model codes were EP0-298K, EP2-298K, EP4-298K, EP6-298K, EP4-333K, EP4-368K, EP/GN0-298K, EP/GN2-298K, EP/GN4-298K, EP/GN6-298K, EP/GN4-333K and EP/GN4-368K. In the model code, the first group of numbers represented water content (%), and the second group of numbers represented environment temperature. For example, EP2-298K represented the pure epoxy model with a water content of 2% at 298 K.

3.3.1. Tensile deformation

The models were stretched in the X direction, and the stretching processes were implemented using the fix deform syntax [50] at a tensile rate of 10^{-5} Å/fs. In the simulation, calculation datas were output every 200 steps.

During the stretching process, the defects in the systems could be defined by changes in atomic

distribution and density [54]. When the material was subjected to tensile stress, the arrangement and distribution of atoms changed, potentially leading to the defects of crack or void.

Take the models EP0-298K and EP/GN0-298K as examples. The snapshots of EP0-298K at the strains of 0, 0.1, 0.2, 0.3 and 0.4 and the density distribution of EP0-298K at the strains of 0, 0.2 and 0.4 are shown in Figures 16 and 17, respectively. The snapshots of EP/GN0-298K at the strains of 0, 0.1, 0.2, 0.3 and 0.4 and the density distribution of EP/GN0-298K at the strains of 0, 0.2 and 0.4 are shown in Figures 18 and 19, respectively. The strain values were chosen based on the relevant literature [1,55,56]. The defects were the irregularities or discontinuities that occurred within the molecular structure. In the schematic illustration of the systems, the voids appeared as areas with sparse atom arrangements, and in the density contour plots, the voids appeared as areas with lower density.

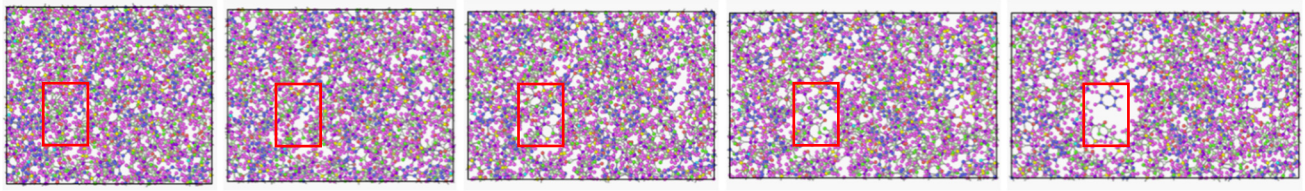

(a) strain = 0.0 (b) strain = 0.1 (c) strain = 0.2 (d) strain = 0.3 (e) strain = 0.4

Figure 16. Schematic illustration of the structural variations of pure epoxy in the tensile process.

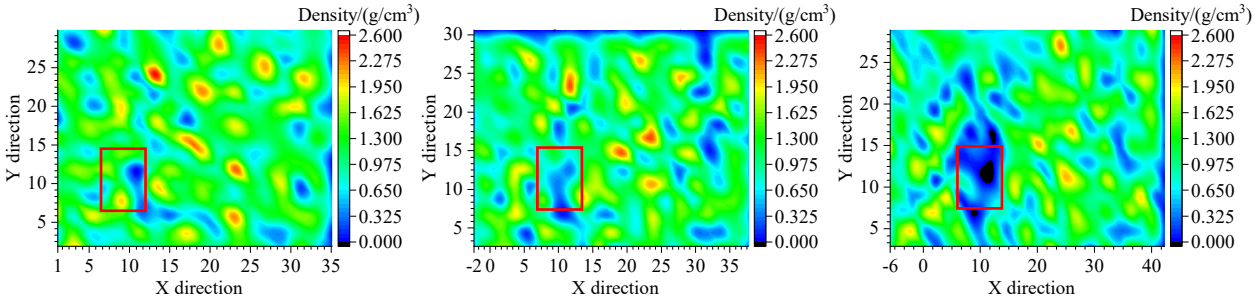

(a) strain = 0.0 (b) strain = 0.2 (c) strain = 0.4

Figure 17. Density contour plots of the molecules in epoxy.

In Figure 16, the changes of the material within the red rectangular frame in the model of EP0-298 were analyzed. It showed that, with the tensile strain increased, the number of atoms in this part decreased, and the defects appeared, at last, inducing the formation of voids. Figure 17 showed that, as the tensile strain increased, the blue color within the red rectangular frame deepened, indicating that the density gradually decreased. Eventually, the color turns black, indicating a density of 0 g/cm^3, which was consistent with the results in Figure 16. Figures 16 and 17 illustrated that when the tensile strain was higher than 0.2, the development rate of defects was relatively fast.

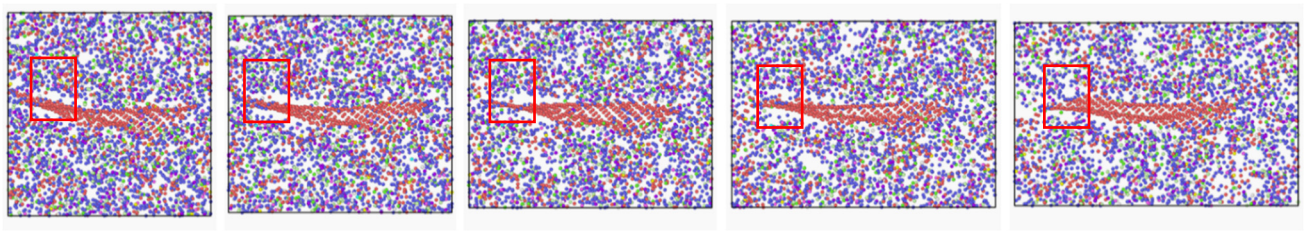

(a) strain = 0.0 (b) strain = 0.1 (c) strain = 0.2 (d) strain = 0.3 (e) strain = 0.4

Figure 18. Schematic illustration of the structural variations of epoxy/graphene in the tensile process.

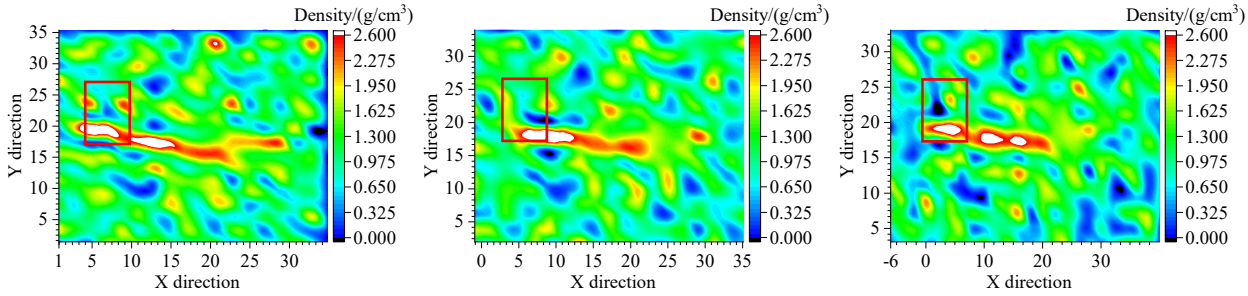

(a) strain = 0.0 (b) strain = 0.2 (c) strain = 0.4

Figure 19. Density contour plots of the molecules in epoxy/graphene.

Figures 18 and 19 indicated that as the tensile strain increased, the internal structure of the epoxy/graphene exhibited similar features to those of epoxy resin. As the tensile deformation of the models increased, the void defects appeared, and continued to develop. When the void defects reached a certain degree or enough voids appeared, some voids defects penetrated, inducing damage to the systems.

Comparing Figures 17 and 19, when the deformation was small, the degrees of defects in pure epoxy and epoxy/graphene were similar. When the deformation was larger, some void defects in pure epoxy connected and formed obvious defects, and the defects developed more rapidly than those in epoxy/graphene.

Due to the high tensile strength and elastic modulus of graphene [17,18], the load on epoxy/graphene could be well transferred to graphene. Moreover, because of the bridging effect of graphene and the strong interaction between graphene and epoxy in epoxy/graphene, when the developing hole defects encountered graphene, they would bypass or cut off the reinforcing material. The addition of graphene reduced the number of defects and inhibited the development of defects, and thus the tensile strength of the epoxy/graphene was enhanced.

3.3.2. Bond length distribution

Material properties were related to their spatial structures, which could be reflected by the bond lengths in the systems. Therefore, the bond length distributions of the models during the tensile process were analyzed.

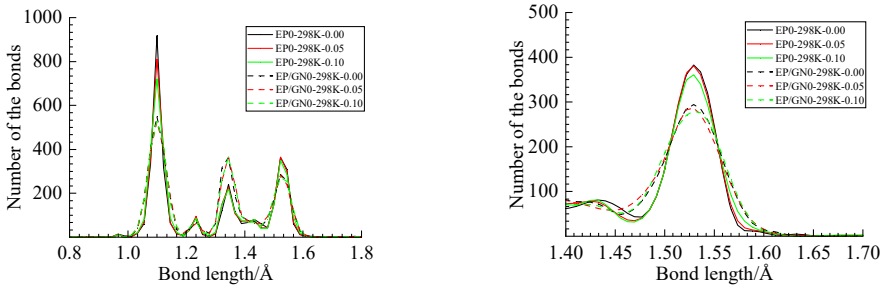

(a) Bond length in the range of 0.8-1.8 Å (b) Bond length in the range of 1.4-1.7 Å

Figure 20. Bond length distribution.

All the bond length distributions of models EP0-298K and EPGN0-298K in the tensile process are shown in Figure 20. The last number in the legends represented the corresponding strain values of the models during the tensile process.

In Figure 20(a), the bond lengths of 1.0–1.2 and 1.2–1.3 Å corresponded to the C-H bonds and C-O bonds. The bond length of 1.3–1.4 Å corresponded to the C-C bonds in the benzene rings and graphene. The bond length of 1.5–1.6 Å mainly corresponded to the rest C-C bonds, which composed the molecular skeletons in the epoxy.

According to Figure 20(b), the C-C bonds in the epoxy backbones were elongated with the increase of tensile deformation; however, the length of the C-C bonds in EP/GN0-298K changed less than that in EP0-298K due to the addition of graphene. On the one hand, the load shared by epoxy in epoxy/graphene composite decreased because the graphene bore part of the load. On the other hand, the defect expansion was inhibited due to the presence of graphene.

3.4. Stress-strain behavior

Every model performed the dynamics simulation of the tensile process three times, and the average value of the calculation results was taken as the final result of the stress-strain curve. The stress-strain curve diagram is shown in Figure 21. The line OA represents the stage of elastic deformation. Point A represents the elastic limit stress. The curve AB represents the stage of inelastic deformation. Point B is the peak point that represents the tensile strength. Post-peak response was the strain softening stage, which was followed by the strain hardening stage [56,57].

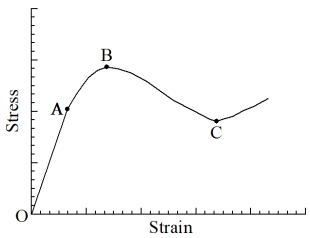

Figure 21. The diagram of stress-strain curve.

3.4.1. Stress-strain behavior of pure epoxy

The tensile stress-strain curves of pure epoxy are illustrated in Figures 22 and 23. The peak stress and its corresponding strain are listed in Table 2. The calculated peak stress of the pure epoxy in the dry environment was 288.6 MPa, which was similar to the calculation results of Xin [58]. The comparison results verified the rationality of the model.

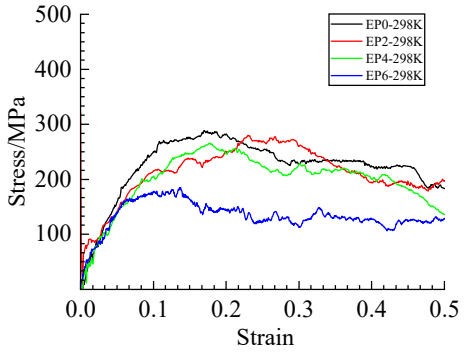

Figure 22. Stress-strain curves of the epoxy with different water contents.

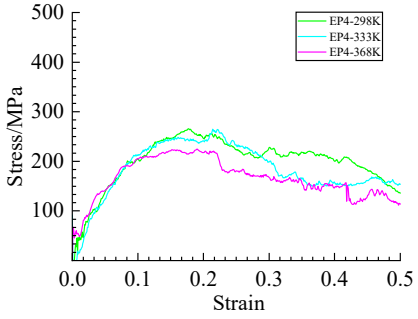

Figure 23. Stress-strain curves of the epoxy at different temperatures.

Table 2. Peak stress and its corresponding strain of the pure epoxy.

Model	stress/GPa	strain
EP0-298K	0.2886	0.1701
EP2-298K	0.2802	0.2302
EP4-298K	0.2660	0.1772
EP6-298K	0.1850	0.1375
EP4-333K	0.2645	0.2142
EP4-368K	0.2246	0.1902

Figure 22 shows the effect of water content on the stress-strain curves of pure epoxy at 298 K. It

could be seen that with the increase of water content, the peak stress of pure epoxy decreased, and the degradation rate of peak stress gradually increased. The peak stress of epoxy with a water content of 2% was close to that of dry epoxy, which illustrated that the water content of 2% had little effect on the tensile strength of pure epoxy. However, the peak strain (strain corresponding to the peak stress) of epoxy with a water content of 2% was obviously higher than that of dry epoxy. This was attributed to the increased hydrogen bonds by the introduction of water molecules, which increased the attraction between molecules and enhanced the deformation ability of the epoxy.

Figure 23 shows the effect of temperature on the stress-strain curves of the models with a water content of 4%. It could be seen that the shapes of the stress-strain curves were similar. The peak stresses of epoxy at temperatures of 298 and 333 K were close, indicating that temperature had little influence on the tensile properties of pure epoxy when the temperature range was 298 to 333 K. At a higher temperature of 368 K, the peak stress of pure epoxy significantly decreased.

3.4.2. Stress-strain behavior of epoxy/graphene

The tensile stress-strain curves of epoxy/graphene are illustrated in Figures 24 and 25. The peak stress and the corresponding strain are listed in Table 3.

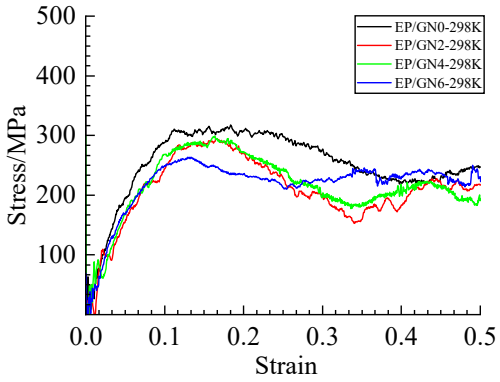

Figure 24. Stress-strain curves of the epoxy/graphene with different water contents.

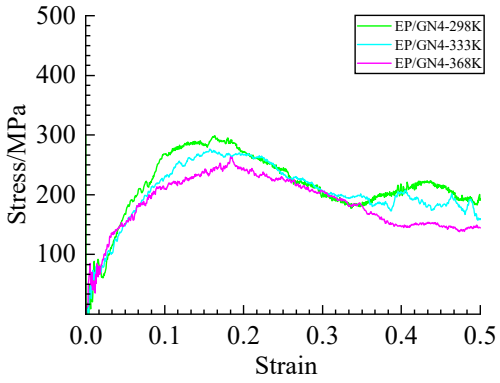

Figure 25. Stress-strain curves of the epoxy/graphene at different temperatures.

Table 3. Peak stress and its corresponding strain of the epoxy/graphene.

Model	stress/GPa	strain
EP/GN0-298K	0.3178	0.1835
EP/GN2-298K	0.2950	0.1650
EP/GN4-298K	0.2989	0.1635
EP/GN6-298K	0.2638	0.1290
EP/GN4-333K	0.2765	0.1575
EP/GN4-368K	0.2635	0.1836

Figure 24 shows the tensile stress-strain curves of epoxy/graphene with different water contents at 298 K. It could be seen that all the curves had similar variation trends, and all of them underwent the stages of elastic deformation, inelastic deformation, strain softening and strain hardening. The research conducted by Li and Strachan [56] and Fard et al. [57] obtained stress-strain curves with similar characteristics. Whether a full stress-strain curve of the material undergoes these four stages is determined by various factors [57].

On the whole, the peak stress of the models decreased as the water content increased. The peak stresses of EP/GN2-298K and EP/GN4-298K were close. When the water content increased to 6%, the peak stress of epoxy/graphene significantly decreased. The stress-strain curves of the models with the water contents of 2 and 4% had more significant decline rates after the peak load than that of the model in a dry environment.

Figure 25 shows the tensile stress-strain curves of epoxy/graphene with a water content of 4% at different temperatures. The peak stress decreased with the increase in temperature. At a higher temperature of 368 K, the stress-strain curve had no obvious strain-hardening stage.

3.4.3. Effect of graphene addition on the stress-strain behavior

The comparison between stress-strain curves of pure epoxy and epoxy/graphene is shown in Figure 26.

The figures indicate that the graphene addition increased the peak stress of the system in the tensile process. Figure 26(a)–(d) shows the comparison of the stress-strain curves of the models at 298 K. It indicated that when the water content was not higher than 4%, the addition of graphene caused the epoxy to undergo an obvious strain hardening stage. When the water content was 6%, the enhancement of graphene on the peak stress of the model was the most obvious. Figure 26(c), (e) and (f) shows the comparison of the stress-strain curves between pure epoxy and epoxy/graphene when the water content was 4%. It indicates that the enhancement of graphene on the peak stress of the model at 298 K was more obvious than that at 333 and 368 K. The comparison results revealed that the improvement effect of graphene on the tensile properties of epoxy was more obvious when in the higher water content and lower temperature environment.

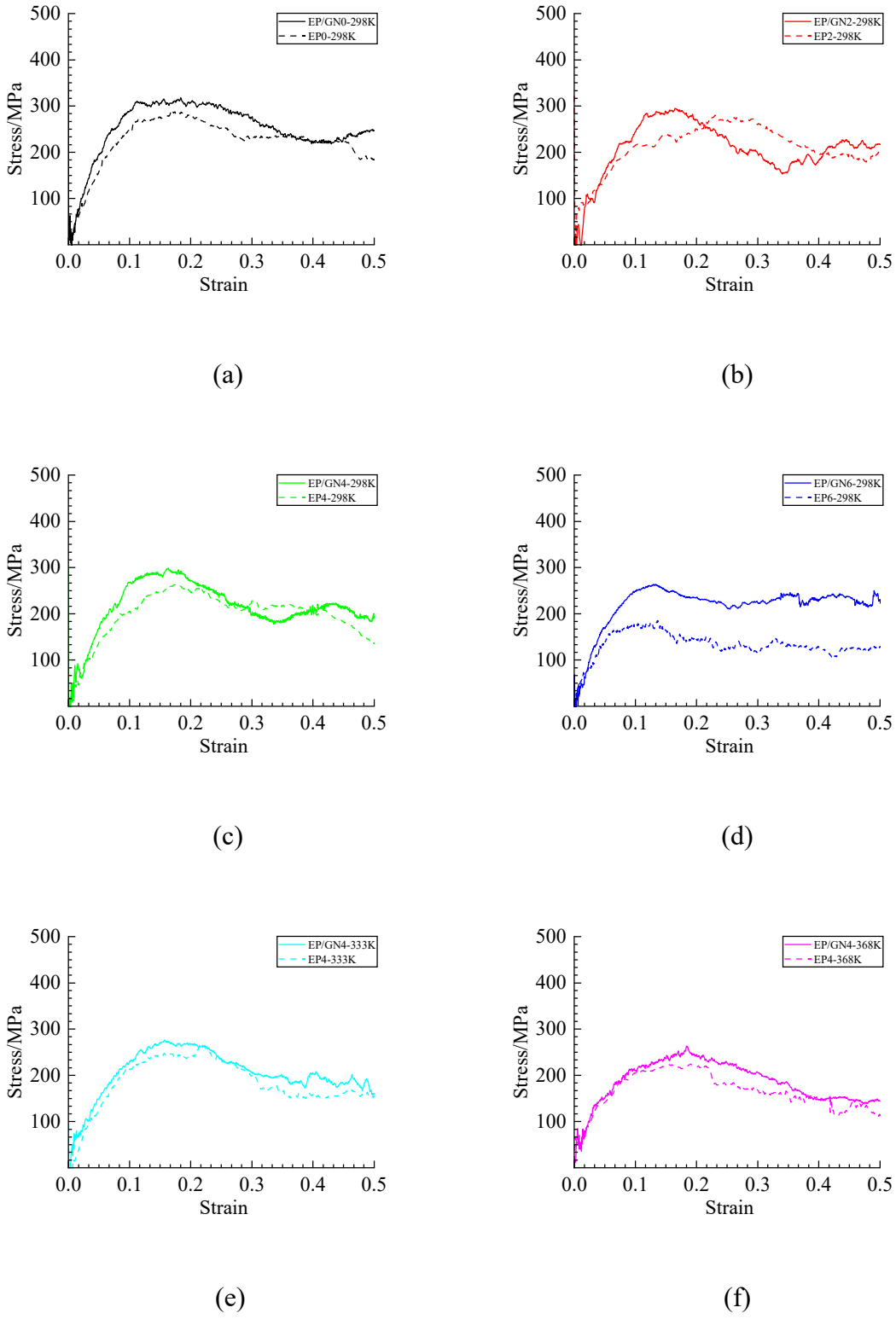

Figure 26. Effect of the graphene addition on the stress-strain curves.

4. Conclusions

The main physical and tensile properties of epoxy/graphene in the hygrothermal environment were investigated at the molecular level, and the conclusions are drawn as follows:

The density and free volume fraction of pure epoxy and epoxy/graphene had similar variation trends with water content. When the water content was less than 2%, the densities of the moist models were lower than that of the dry model, and the free volume fractions of moist models were higher than that of the dry model. This was due to the addition of water molecules introducing hydrogen bonds, and the beneficial effect of hydrogen bonds was more obvious than the plasticizing effect of water molecules on the epoxy. When the water content was higher than 2%, the physical performance degraded as the water content increased.

The MSD of water molecules in pure epoxy and epoxy/graphene increased as the water content and temperature increased. When the water content was not higher than 4%, and the temperature was not higher than 333 K, the addition of graphene had little effect on the diffusion rate of water molecules. When the water content was higher than 4% or the temperature was higher than 333 K, the addition of graphene could significantly improve the barrier performance of epoxy to water molecules, thereby reducing the diffusion rate of water molecules in epoxy and enhancing the stability of the system.

The introduced graphene shared the load borne by the epoxy, which increased the crack strain value of the epoxy, delayed the expansion of defects in the epoxy, and improved the deformation performance of the epoxy. This demonstrated that the deformation mechanisms of pure epoxy and epoxy/graphene were different.

On the whole, with the increase in water content or temperature, the peak stress of pure epoxy and epoxy/graphene decreased. The stress-strain curves of pure epoxy had no obvious strain-hardening stage. However, when the temperature was less than 368 K, the stress-strain curves of epoxy/graphene showed an obvious strain-hardening stage at the tensile strain value of 0.3–0.4.

Acknowledgments

This research was supported by the research program of Beijing Building Materials Testing Academy Co., Ltd (KYJC013).

Conflict of interest

The authors declare there is no conflict of interest.

References

1. D. Xin, Q. Han, A molecular dynamics investigation on the compression of cross-linked epoxy resins, *Mol. Simul.*, **41** (2015), 1509–1514. https://doi.org/10.1080/08927022.2014.994623
2. L. Shen, L. Zou, M. Ding, T. Zhao, L. Zhang, Q. Li, Molecular dynamics simulation on dielectric constant and thermal conductivity of crosslink epoxy/functionalized graphene nano-composites, in *IOP Conference Series: Materials Science and Engineering*, **761** (2020), 012009. https://doi.org/10.1088/1757-899X/761/1/012009
3. W. Sun, S. Yu, S. Gao, X. Yao, H. Xu, B. Qian, et al., Molecular dynamics simulation of water molecule diffusion in graphene-reinforced epoxy resin anticorrosive coatings, *J. Chin. Soc. Corros. Prot.*, **41** (2021), 411–416. https://doi.org/10.11902/1005.4537.2020.227

4. Y. Li, S. Wang, Q. Wang, A molecular dynamics simulation study on enhancement of mechanical and tribological properties of polymer composites by introduction of graphene, *Carbon*, **111** (2017), 538–545. http://doi.org/10.1016/j.carbon.2016.10.039
5. Q. Xie, K. Fu, S. Liang, B. Liu, L. Lu, X. Yang, et al., Micro-structure and thermomechanical pproperties of crosslinked epoxy composite modified by nano-SiO2: A molecular dynamics simulation, *Polymers (Basel)*, **10** (2018), 801. https://doi.org/10.3390/polym10070801
6. Y. Yang, G. Xian, H. Li, L. Sui, Thermal aging of an anhydride-cured epoxy resin, *Polym. Degrad. Stab.*, **118** (2015), 111–119. https://doi.org/10.1016/j.polymdegradstab.2015.04.017
7. D. Li, *Evolution of the Properties of an Epoxy Resin Submitted to Water and Alkaline Immersion and the molecular Dynamic Simu*lation, Master's thesis, Harbin Institute of Technology in Harbin, 2015.
8. Y. Xiao, G. Xian, Effects of moisture ingress on the bond between carbon fiber and epoxy resin investigated with molecular dynamics simulation, *Polym. Compos.*, **39** (2018), E2074–E2083. https://doi.org/ 10.1002/pc.24459
9. F. Zhao, H. Ba, X. Gao, The durability of epoxy resin coating, *J. Wuhan Univ. Technol. Mater. Sci. Ed.*, **23** (2008), 242–244. https://doi.org/10.1007/s11595-006-2242-z
10. J. Arias, M. M. Escobar, C. Bernal, A. Vázquez, Aging in water and in an alkaline medium of unsaturated polyester and epoxy resins: experimental study and modeling, *Adv. Polym. Technol.*, **37** (2018), 450–460. https://doi.org/10.1002/adv.21684
11. A. Uthaman, G. Xian, S. Thomas, Y. Wang, Q. Zheng, X. Liu, Durability of an epoxy resin and its carbon fiber-reinforced polymer composite upon immersion in water, acidic, and alkaline solutions, *Polymers (Basel)*, **12** (2020), 614. https://doi.org/10.3390/polym12030614
12. B. Wang, D. Li, G. Xian, C. Li, Effect of Immersion in water or alkali solution on the structures and properties of epoxy resin, *Polymers (Basel)*, **13** (2021), 1902. https://doi.org/10.3390/polym13121902
13. F. Jeyranpour, G. Alahyarizadeh, H. Minuchehr, The thermo-mechanical properties estimation of fullerene-reinforced resin epoxy composites by molecular dynamics simulation-A comparative study, *Polymer*, **88** (2016), 9–18. https://doi.org/10.1016/j.polymer.2016.02.018
14. Y. Zhang, J. Ma, C. Wu, X. Han, W. Zhang, Effects of moisture ingress on the mesoscale mechanical properties of epoxy adhesives under elevated temperature, *Polym. Test.*, **94** (2021), 107049. https://doi.org/10.1016/j.polymertesting.2020.107049
15. H. Chai, X. Wang, W. U. Rehman, X. Yang, T. Meng, Study on water absorption and mechanical properties of CNF-Ti reinforced epoxy resin composites, *Plast., Rubber Compos.*, **52** (2021), 47–58. https://doi.org/10.1080/14658011.2021.2017127
16. P. Penjumras, R. A. Rahman, R. A. Talib, K. Abdan, Mechanical properties and water absorption behaviour of durian rind cellulose reinforced poly (lactic acid) biocomposites, *Int. J. Adv. Sci. Eng. Inf. Technol.*, **5** (2015), 343–349. https://doi.org/10.18517/ijaseit.5.5.574
17. A. King, G. Johnson, D. Engelberg, W. Ludwig, L. Marrow, Observations of intergranular stress corrosion cracking in a grain-mapped polycrystal, *Science*, **321** (2008), 382–385. https://doi.org/10.1126/science.abq1274
18. X. Sun, H. Sun, H. Li, H. Peng, Developing polymer composite materials: carbon nanotubes or graphene?, *Adv. Mater.*, **25** (2013), 5153–5176. https://doi.org/10.1002/adma.201301926

19. L. C. O. Silva, G. G. Silva, P. M. Ajayan, B. G. Soares, Long-term behavior of epoxy/graphene-based composites determined by dynamic mechanical analysis, *J. Mater. Sci.*, **50** (2015), 6407–6419. https://doi.org/10.1007/s10853-015-9193-8
20. W. Hou, Y. Gao, J. Wang, D. J. Blackwood, S. Teo, Recent advances and future perspectives for graphene oxide reinforced epoxy resins, *Mater. Today Commun.*, **23** (2020), 100883. https://doi.org/10.1016/j.mtcomm.2019.100883
21. Y. Ni, L. Chen, K. Teng, J. Shi, X. Qian, Z. Xu, et al., Superior mechanical properties of epoxy composites reinforced by 3D interconnected graphene skeleton, *ACS Appl. Mater. Interfaces*, **7** (2015), 11583–11591. https://doi.org/10.1021/acsami.5b02552
22. T. Hu, D. Zhao, C. Cheng, S. Meng, Z. Ding, L. Wu, Preparation and mechanical properties of graphene oxide reinforced epoxy composites, *J. Beijing Univ. Chem. Technol. (Nat. Sci. Ed.)*, **45** (2018), 29–33. https://doi.org/10.13543/j.bhxbzr.2018.06.005
23. W. Xiao, Y. Liu, S. Guo, Composites of graphene oxide and epoxy resin assuming a uniform 3D graphene oxide network structure, *RSC Adv.*, **6** (2016), 8694–8698. https://doi.org/10.1039/c6ra16335a
24. H. Yao, S. A. Hawkins, H. Sue, Preparation of epoxy nanocomposites containing well-dispersed graphene nanosheets. *Compos. Sci. Technol.*, **146** (2017), 161–168. https://doi.org/10.1016/j.compscitech.2017.04.026
25. S. A. Bansal, A. P. Singh, A. Kumar, S. Kumar, N. Kumar, J. K. Goswamy, Improved mechanical performance of bisphenol-A graphene-oxide nano-composites, *J. Compos. Mater.*, **52** (2018), 2179–2188. https://doi.org/10.1177/0021998317741952
26. B. Hu, Y. Cong, B. Zhang, L. Zhang, Y. Shen, H. Huang, Enhancement of thermal and mechanical performances of epoxy nanocomposite materials based on graphene oxide grafted by liquid crystalline monomer with Schiff base, *J. Mater. Sci.*, **55** (2020), 3712–3727. https://doi.org/10.1007/s10853-019-04273-2
27. Y. Zhang, D. Zhang, X. Wei, S. Zhong, J. Wang, Enhanced tribological properties of polymer composite coating containing graphene at room and elevated temperatures, *Coatings*, **8** (2018), 91. https://doi.org/10.3390/coatings8030091
28. A. Wolk, M. Rosenthal, J. Weiss, M. Voigt, J. Wesendahl, M. Hartmann, et al., Graphene oxide as flexibilizer for epoxy amine resins, *Prog. Org. Coat.*, **122** (2018), 280–289. https://doi.org/10.1016/j.porgcoat.2018.05.028
29. S. C. Her, L. Y. Chen, Fabrication and characterization of graphene/epoxy nanocomposites, *Mater. Sci.*, **25** (2019), 433–440. https://doi.org/10.5755/j01.ms.25.4.19462
30. P. Bian, W. Verestek, S. Yan, X. Xu, H. Qing, S. Schmauder, A multiscale modeling on fracture and strength of graphene platelets reinforced epoxy, *Eng. Fract. Mech.*, (2020), 107197. https://doi.org/10.1016/j.engfracmech.2020.107197
31. P. Bian, S. Schmauder, H. Qing, Strength and damage of nanoplatelets reinforced polymer: A 3D finite element modeling and simulation, *Compos. Struct.*, **245** (2020), 112337. https://doi.org/10.1016/j.compstruct.2020.112337
32. A. Yadav, A. Kumar, P. K. Singh, K. Sharma, Glass transition temperature of functionalized graphene epoxy composites using molecular dynamics simulation, *Integr. Ferroelectr.*, **186** (2018), 106–114. https://doi.org/10.1080/10584587.2017.1370331

33. A. Salehi, S. Rash-Ahmadi, Effect of adsorption, hardener, and temperature on mechanical properties of epoxy nanocomposites with functionalized graphene: A molecular dynamics study, *J. Mol. Graphics Modell.*, **117** (2022), 108311. https://doi.org/10.1016/j.jmgm.2022.108311
34. O. Starkova, S. Gaidukovs, O. Platnieks, A. Barkane, K. Garkusina, E. Palitis, et al., Water absorption and hydrothermal ageing of epoxy adhesives reinforced with amino-functionalized graphene oxide nanoparticles. *Polym. Degrad. Stab.*, **191** (2021), 109670. https://doi.org/10.1016/j.polymdegradstab.2021.109670
35. S. Prolongo, A. Jiménez-Suárez, R. Moriche, A. Ureña, Influence of thickness and lateral size of graphene nanoplatelets on water uptake in epoxy/graphene nanocomposites, *Appl. Sci.*, **8** (2018), 1550. https://doi.org/10.3390/app8091550
36. W. Li, L. Zhang, M. Zhang, S. Chen, Structures of graphene-reinforced epoxy coatings and the dynamic diffusion of guest water: a molecular dynamics study, *Ind. Eng. Chem. Res.*, **59** (2020), 20749–20756. https://doi.org/10.1021/acs.iecr.0c04673
37. L. Zhu, C. Feng, Y. Cao, Corrosion behavior of epoxy composite coatings reinforced with reduced graphene oxide nanosheets in the high salinity environments, *Appl. Surf. Sci.*, **493** (2019), 889–896. https://doi.org/10.1016/j.apsusc.2019.06.271
38. L. Yao, J. Zhao, Mechanism study of doped graphene on improving mechanical properties and corrosion resistance of epoxy resin, *J. At. Mol. Phys.*, **38** (2021), 131–135. https://doi.org/10.19855/j.1000-0364.2021.016003
39. P. Bian, H. Qing, A phase-field based finite element method for modeling graphene flake reinforced composites, *Mech. Adv. Mater. Struct.*, (2022), 1–16. https://doi.org/10.1080/15376494.2022.2048146
40. P. L. Bian, H. Qing, S. Schmauder, A novel phase-field based cohesive zone model for modeling interfacial failure in composites, *Int. J. Numer. Methods Eng.*, (2021), 1–24. https://doi.org/10.1002/nme.6821
41. W. Li, W. Chai, L. Zhang, Y. Guo, W. Wang, S. Chen, Atomic insight into the influences of moisture ingress on the structures and dynamics of graphene-epoxy interfaces, *Compos. Sci. Technol.*, **219** (2022), 109222. https://doi.org/10.1016/j.compscitech.2021.109222
42. C. Sheng, G. Wu, X. Sun, S. Liu, Molecular dynamics investigation of the thermo-mechanical properties of the moisture invaded and cross-linked epoxy system, *Polymers (Basel)*, **14 (**2022), 103, https://doi.org/10.3390/polym14010103
43. J. Fan, P. Li, Z. Wang, J. Yang, The temperature-dependent properties of epoxy-functionalized graphene oxide/epoxy nanocomposites: insights from simulation and experiment, *J. Mater. Sci.*, **57** (2022), 15298–15313, https://doi.org/10.1007/s10853-022-07575-0
44. K. Fu, Q. Xie, F. LÜ, Q. Duan, X. Wang, Q. Zhu, et al., Molecular dynamics simulation and experimental studies on the thermomechanical properties of epoxy resin with different anhydride curing agents, *Polymers (Basel)*, **11** (2019), 975, https://doi:10.3390/polym11060975
45. B. S. Sindu, S. Sasmal, Evaluation of mechanical characteristics of nano modified epoxy based polymers using molecular dynamics, *Comput. Mater. Sci.*, **96** (2015), 146–158, http://dx.doi.org/10.1016/j.commatsci.2014.09.003
46. Q. Yang, X. Yang, X. Li, L. Shi, G. Sui, The curing and thermal transition behavior of epoxy resin: a molecular simulation and experimental study, *RSC Adv.*, **3** (2013), 7452–7459. https://doi.org/10.1039/c3ra40699g

47. C. Sheng, G. Wu, X. Sun, S. Liu, Molecular dynamics investigation of the thermo-mechanical properties of the moisture invaded and cross-linked epoxy system, *Polymers (Basel)*, **14** (2022), 103. https://doi.org/10.3390/polym14010103
48. S. Ma, P. Chen, J. Xu, X. Xiong, Molecular dynamics simulations of key physical properties and microstructure of epoxy resin cured with different curing agents, *J. Mater. Sci.*, **57** (2022), 1123–1133. https://doi.org/10.1007/s10853-021-06799-w
49. Y. Jin, X. Han, P. Hu, *Modelling and Experimental Study on Diffusion Characteristics of Epoxy Adhesive Immersed in Aqueous Environment*, The 26th Annual Conference of Beijing Adhesion Society, Beijing, 2017.
50. K. Li, *Molecular Dynamic Simulations of Crosslinked Epoxy Resin and Properties of Nano-Composites Containing Phenyl POSS*, Ph.D thesis, Beijing University of Chemical Technology, Beijing, 2017.
51. Y. Liu, *Research on the Aging Properties of Epoxy Resin in Hygrothermal Environment*, Master's thesis, Chongqing University in Chongqing, 2018
52. R. Cai, J. Zhao, N. Lv, A. Fu, C. Yin, C. Song, et al., Curing and molecular dynamics simulation of MXene/Phenolic epoxy composites with different amine curing agent systems, *Nanomaterials*, **12** (2022), 2249. https://doi.org/10.3390/nano12132249
53. Y. Xie, H. Lei, H. Huang, H. Pan, S. Zhao, Y. Liu, et al., Molecular simulation on hygrothermal ageing process of epoxy resin, *Insul. Mater.*, **52** (2019), 70–77. https://doi.org/10.16790/j.cnki.1009-9239.im.2019.09.013
54. H. Yan, Z. Wang, F. Sun, R. Gao, Y. Fu, Molecular dynamics simulation of crosslinked epoxy resin tensile properties, *Eng. Plast. Appl.*, **50** (2022), 113–117, https://doi.org/10.3969/j.issn.1001-3539.2022.12.019
55. S. Yang, J. Qu, Computing thermomechanical properties of crosslinked epoxy by molecular dynamic simulations, *Polymer*, **53** (2012), 4806–4817, http://dx.doi.org/10.1016/j.polymer.2012.08.045
56. C. Li, A. Strachan, Molecular dynamics predictions of thermal and mechanical properties of thermoset polymer EPON862/DETDA, *Polymer*, **52** (2011), 2920–2928, https://doi:10.1016/j.polymer.2011.04.041
57. M. Y. Fard, Y. Liu, A. Chattopadhyay, Characterization of epoxy resin including strain rate effects using digital image correlation system, *J. Aerosp. Eng.*, **25** (2012), 308–319. http://dx.doi.org/10.1061/(ASCE)AS.1943-5525.0000127
58. D. Xin, *Mechanical Properties and the Interface Failure Mechanism of Epoxy Resin under Hygrothermal Condition*, Ph.D thesis, South China University of Technology, Guangzhou, 2013.

AIMS Press